AG-336



# 6. BLUFF-BODY BLOCKAGE CORRECTIONS IN CLOSED- AND OPEN-TEST-SECTION WIND TUNNELS

AUTHOR : KEVIN COOPER

PAGE

## LIST OF SYMBOLS

| | |
|---|---|
| $B$ | Single or duplex tunnel width. For model reflected about the ground plane (duplex), $B = 2H_t$ |
| $B_t$ | tunnel width |
| $C$ | duplex test-section area, $2C_t$ or $2C_n$ |
| $C_c$ | open tunnel single or duplex collector area |
| $C_t$ | closed tunnel test section area |
| $C_n$ | open tunnel test section area |
| $C_{Dc}$ | blockage-corrected, wind-axis drag coefficient |
| $C_{DcM1}$ | wind-axis drag coefficient corrected by Maskell's method, eqn. (6.3) |
| $C_{DcM2}$ | wind-axis drag coefficient corrected by Hackett's two-step version of Maskell, eqn. (6.14) |
| $C_{Di}$ | induced-drag coefficient |
| $C_{Do}$ | drag due to skin friction coefficient |
| $C_{Dr}$ | support rig (strut) drag |
| $C_{Du}$ | uncorrected, wind-axis drag coefficient |
| $C_{Duo}$ | uncorrected, wind-axis drag coefficient at zero yaw angle |
| $C_{Dus}$ | uncorrected, separated-flow drag |
| $C_{D\infty}$ | drag coefficient corrected for blockage only, excluding wake constraint, eqn. (6.13) |
| $C_{Du,vis}$ | viscous component of drag, $(C_{Do} + C_{Dus}) = (C_{Du} - C_{Di})$ |
| $C_L$ | lift coefficient |
| $C_Y$ | side force coefficient |
| $C_{pbc}$ | corrected base pressure coefficient |
| $C_{pbu}$ | uncorrected base pressure coefficient |
| $F$ | duplex model projected frontal area, $2(S_m \cos\psi + S_Y \sin\lvert\psi\rvert)$, eqn. (6.19) |
| $H$ | single or duplex tunnel height. For model reflected about the ground plane (duplex), $H = B_t$ |
| $H_t$ | tunnel height |
| $K$ | empirical solid blockage constant for automobiles determined by Mercker, 1.0 |
| $L_m$ | model length |
| $L_p$ | projected length of model, $L_m \cos\psi + w_m \sin\lvert\psi\rvert$ |
| $L_{ts}$ | test section length |
| $m$ | Cowdrey's empirical blockage constant, eqn. (6.7) |
| $m'$ | Cowdrey's empirical blockage constant, eqn. (6.9) |
| $Q_s$ | source strength used in an open-jet tunnel to calculate nozzle interference due to a model |
| $r$ | radial co-ordinate |
| $R_c$ | hydraulic diameter of single or duplex open tunnel collector |
| $R_n$ | hydraulic diameter of single or duplex open tunnel nozzle |
| $S$ | single or duplex model frontal area, as appropriate |
| $S_m$ | model frontal area |
| $S_Y$ | model side area |
| $S_b$ | model base area (area of separated-flow area on base) |
| $T$ | blockage constant = $\tau\sqrt{\pi}/2 = 0.36(B/H+H/B)$ |
| $U_o$ | measured, upstream reference velocity not influenced by blockage |

| | |
|---|---|
| $U_c$ | blockage-corrected reference velocity |
| $U_m$ | measured, upstream reference velocity influenced by blockage |
| $U_n$ | open-jet reference velocity measured using a nozzle reference static pressure |
| $\bar{U}_n$ | average velocity over the nozzle exit plane of an open-jet tunnel with a model present |
| $U_p$ | open-jet reference velocity measured using a plenum chamber reference static pressure |
| $U_{wa}$ | velocity including attached-flow wake blockage |
| $U_{wc}$ | velocity including collector-plane wake blockage |
| $U_{ws}$ | velocity including separated-flow wake blockage |
| $U_x(x,r)$ | total velocity due to point source at location (x,r) |
| $u_x(x,r)$ | incremental velocity due to source at (x,r) |
| $V$ | single or duplex model volume, as appropriate |
| $V_m$ | model volume |
| $V_e$ | effective model volume, $1.75V_m$ |
| $V_t$ | variable portion of test section volume, $L_pC$ |
| $w_m$ | model width |
| $x$ | longitudinal position, positive downstream from reference point |
| $\Delta C_D$ | incremental drag, $(C_{Du} - C_{Dc})$ |
| $\Delta C_{DM}$ | drag increment due to separated-flow wake constraint |
| $\Delta C_{DHB}$ | buoyancy drag increment due to empty tunnel longitudinal pressure gradient |
| $\Delta C_{Dwb}$ | buoyancy drag increment due to wake constraint |
| $\Delta C_{Dwi}$ | drag increment due to the wake constraint |
| $\Delta U_{wa}$ | velocity increment due to attached-flow wake blockage, $(U_{wa} - U_o)$ |
| $\Delta U_{ws}$ | velocity increment due to separated-flow wake blockage, $(U_{ws} - U_o)$ |
| $\varepsilon$ | total blockage factor at the model location, $(U_c - U_o)/U_o$ |
| $\varepsilon_c$ | collector blockage factor at the model location |
| $\varepsilon_d$ | attenuated blockage factor downstream of model centre, eqn. (6.22) |
| $\varepsilon_n$ | nozzle blockage factor at the model location |
| $\varepsilon_{qn}$ | nozzle blockage factor at the nozzle plane |
| $\varepsilon_p$ | plenum blockage factor at the model location |
| $\varepsilon_{qp}$ | plenum blockage factor at the nozzle plane |
| $\varepsilon_s$ | solid blockage factor at the model location, $(U_s - U_o)/U_o$ |
| $\varepsilon_u$ | attenuated blockage factor upstream of model centre, eqn. (6.21) |
| $\varepsilon_w$ | wake blockage factor at the model location, $(U_w - U_o)/U_o$ |
| $\varepsilon_{wc}$ | wake-blockage factor at the collector plane, $(U_{wc} - U_o)/U_o$ |
| $\varepsilon_{wa}$ | attached-flow, wake blockage factor at the model location, $(U_{wa} - U_o)/U_o$ |
| $\varepsilon_{ws}$ | separated-flow, wake blockage factor at the model location, $(U_{ws} - U_o)/U_o$ |
| $\eta$ | Mercker's empirical wake blockage constant, 0.41; eqn. (6.19) |
| $\theta$ | Maskell's separated-flow wake-blockage constant |
| $\tau$ | solid blockage constant, $= 2T/\sqrt{\pi} = 0.41(B/H + H/B)$ |
| $\psi$ | yaw angle |

# 6.1 INTRODUCTION

## 6.1.1 HISTORY AND STATUS

The effects of the constraints imposed by wind tunnel test section boundaries on the flows around bluff bodies - those bodies having leading-edge separation without re-attachment or having large regions of separated flow further aft on the body - are even now not fully understood. The physics of the interaction of the boundaries of a wind tunnel test section on these wake flows was explored by Maskell [1, 2], based on an analysis of measurements made on three-dimensional flat plates mounted normal to the flow. His results demonstrated that the wall constraint in closed test sections was five times greater than predicted by the classical derivations for bodies with thin wakes. It was clear that large separated flows from stalled wings and bluff bodies must be treated differently than the attached-flow cases.

The impetus for Maskell's development was the need to understand the differences between measurements made on slender delta wings in different wind tunnels. Using normal-flat-plate measurements to develop the flow physics, Maskell was able to generalise these results to the separated-wing case. His derivation was predicated on the principle that the pressure distribution was invariant under constraint, meaning that the pressure field was only scaled by a constant speed increase in the presence of the constraining solid test section walls.

Since this first development for wing flows, the families of separated-flow shapes that have come under common study in the wind tunnel have increased. In particular, the sciences of wind engineering and surface vehicle aerodynamics have advanced rapidly. The aerodynamic loading and stability of bridges and tall buildings is a governing factor in their design while the efficient aerodynamic development of surface vehicles is of major importance in the areas of energy conservation, handling and noise. It is now standard practice to use wind tunnel studies to demonstrate the stability of long-span, cable-supported bridges, to measure the mean and unsteady loads on tall buildings, and to measure and improve the aerodynamic characteristics of surface vehicles. In the latter case, large wind tunnels of open and closed test sections are used routinely for full-scale road vehicle development. An obvious benefit of the availability of proven blockage-correction methods is the ability to minimise the size of the full-scale facility. Another reason for needing an accurate test speed correction method is to provide accurate speed setting during measurement of the sound pressure levels of road vehicles, which vary with the fourth to the sixth power of velocity. This point is particularly pertinent at the time of writing, when approximately one-half of all full-scale passenger car wind tunnel testing is utilised for wind-noise assessment and improvement.

In recent years, the major developments in wall corrections for bluff shapes have come through the development of boundary-measurement-based methods. Here, the mathematical models that are used to represent the bodies in the test section are sufficiently general to extend to both bluff and streamlined shapes. These methods are demanding of instrumentation and computing time. In many cases, the methods are not available or are too demanding for routine use, so there remains a continuing need for simple, analytically-based approximations to the bluff-body blockage effect.

### 6.1.2 Closed and Open Test Sections

Both closed and open test sections are commonly used for studies of all the geometries mentioned above. In general, the closed-wall test section predominates in North America and the United Kingdom for automotive and bluff-body testing, while open-jet test sections are prevalent in Europe. The closed test section requires a larger correction, but has the benefit of precisely defined boundaries and a long test section. The open test section has a solid blockage effect of opposite sign to, and of smaller magnitude than, that of the closed test section. There is no velocity increment at the model due to the constrained wake for the open test section although there is a wake effect that changes the drag.

It has been recognised [3] that additional interference effects may occur on a bluff body in the short test section typical of open tunnels. These effects are not accounted for in the classical theories. The physics of corrections in closed test sections are the better developed because the need was evident - the corrections were known to be large, especially for bluff shapes. The development of open-test-section corrections has lagged, in part because they were small, or thought to be small. However, this assumption has been shown to be incorrect for bluff automotive shapes and has lead to increased activity in the European automotive wind tunnels to understand the effects and to derive appropriate corrections for them [4].

### 6.1.3 Important Test Section Boundaries

In the classical aeronautical derivations discussed in the earlier chapters, the important test section boundaries were the lateral boundaries - the side walls, floor and ceiling of the closed tunnel or the free-jet shear layer of the open tunnel. When a body under study has a large separated wake, the proximity of the end of the test section to the base of the model has an effect that reduces the measured drag. Further, high-drag bluff bodies have larger upstream flow-displacement effects in the test section than streamlined bodies have. These effects can interact with the pressure taps used to measure the static reference pressure at the entrance to the test section in open and closed tunnels, and can distort the flow leaving the nozzle of an open tunnel.

### 6.1.4 Comparison of Closed and Open Test Sections

As an introduction to the relative distortions produced in the two major test-section types, it is useful to compare the influences of solid-wall and free-jet boundaries on measurements on simple bluff bodies.

A typical comparison is presented in Figures 6.1 and 6.2, utilising data [5, 6, 7, 8] measured for normal flat plates and for various rectangular blocks, both wall-mounted and centrally-mounted in the test section. Figure 6.1 shows typical drag coefficient variations with model size and type. As expected, the closed test sections show a drag increase with model area while the open test sections show a drag reduction. The blockage effect in the open test section is less than in the closed test section, but the difference between open and closed is not as large as would be found for streamlined models. The slopes of the drag-blockage curves in the closed test sections are greater for the model families having higher drag. The drag data for the block model in the closed tunnel fall into a family of nearly parallel curves with yaw angle as the parameter, as seen in Figure 6.1.

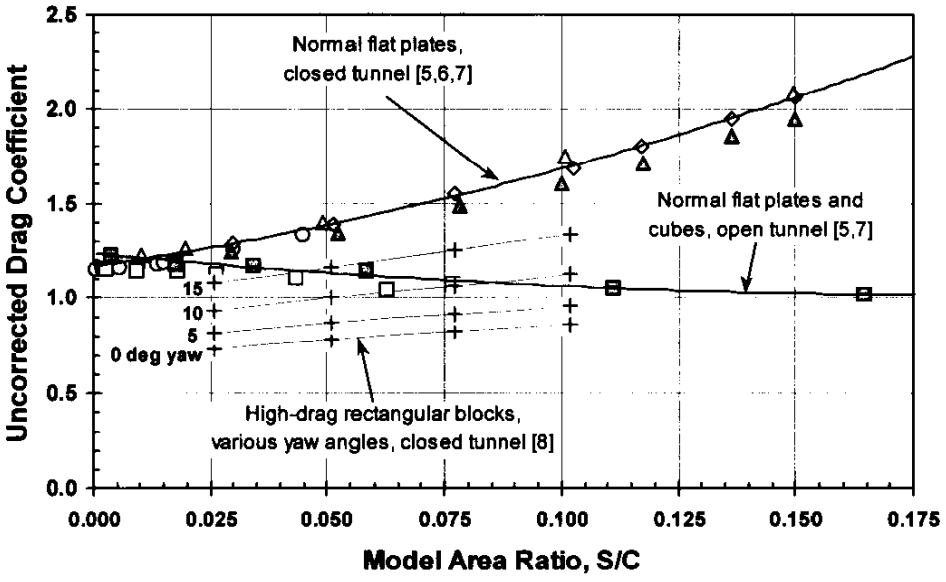


Fig. 6.1: Bluff-Body Blockage Effects on Measured Drag in Closed and Open Test Sections [5, 6, 7, 8]

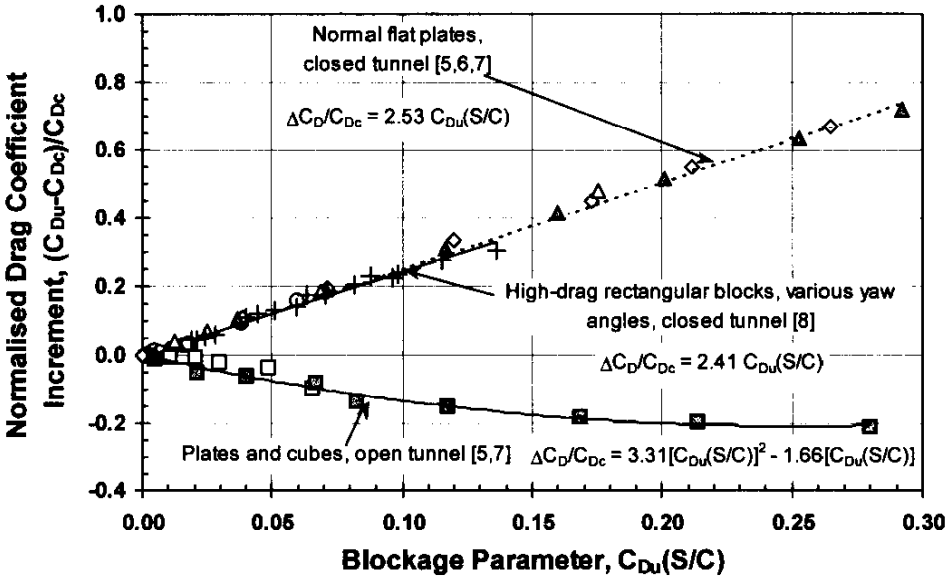


Fig. 6.2: Collapse of Normalised Drag Increments Due to Blockage in Closed and Open Test Sections [5, 6, 7, 8]

Figure 6.2 re-plots the data from Figure 6.1, presenting the normalised incremental drag change due to blockage, $(\Delta C_D / C_{Dc}) = (C_{Du} - C_{Dc})/C_{Dc}$, as a function of the drag in the test section, given by the blockage parameter $C_{Du}(S/C)$. The corrected flat plate drag coefficients were determined by fitting the measured data with least squares, second-order polynomials. The rectangular block data were fitted with second-order polynomials having zero slopes at the origin. The data are now grouped primarily by wind tunnel test section type, with little difference due to model type. The dependence on yaw angle of the data for the block model in the closed test section has disappeared. The blockage effect on the plates in

the open test section, in the linear region at smaller blockage, is about 65% of that in the closed test section. It would appear that the boundary effects in the open test section are significantly larger than would be predicted from classical aerodynamic theory. The expression "boundary effects", rather than "blockage effects" was purposefully chosen because the observed drag distortion is strongly influenced by the finite length of the free jet.

## 6.2 METHODS FOR CLOSED TEST SECTIONS

The early classical boundary-correction theories were small-disturbance analyses. These theories assumed that the models were small in the test section, that the drag coefficients were small and primarily due to skin friction, that wakes were thin and that no flow separations existed. Growing requirements for bluff-body testing necessitated an extension of the classical theories to cater for these cases, examples of which were the stalled wing and the defining case, the flat plate normal to the flow. A summary of blockage corrections for bluff bodies can be found in [9].

### 6.2.1 MASKELL'S ANALYSIS

The founding approach to the estimation of the wake blockage of bluff models in closed test sections was that of Maskell [1]. He applied conservation of momentum and physical arguments supported by wind tunnel measurements on normal flat plates [10] to formulate a theory for the wake blockage produced by separated flows. The assumptions made by Maskell were:

1. that the pressure distribution was invariant under wall constraint,
2. that separated flows from three-dimensional bodies tended to become axially symmetric far downstream,
3. that the base pressure was constant over the separated region and was equal to the static pressure on the wake boundary,

After application of these assumptions, momentum theory led to a dynamic pressure correction of the form,

$$\left(\frac{q_c}{q_u}\right)=\left(\frac{C_{Du}}{C_{D\infty}}\right)=1+\theta C_{D\infty}(S/C) \tag{6.1}$$

where:

$$\theta=-1/C_{pbc} \tag{6.2}$$

$C_{pbc}$ is the corrected base pressure coefficient and $C_{D\infty}$ is the drag coefficient corrected for blockage but not corrected for wake distortion due to the test section walls. Equation (6.1), requires iteration since the magnitude of the correction depends on the corrected drag coefficient. Maskell made a fourth assumption to include the effect of the walls on the shape of the wake boundary. He assumed

4. that the constraining effect of the test section walls reduced the expansion of the wake and that this reduction was in proportion to the contraction of the external stream around the wake.

The final form of the separated-flow component of the wake-blockage correction equation then became,

$$\left(\frac{q_c}{q_u}\right)=\left(\frac{C_{Du}}{C_{DcM1}}\right)=1+\theta C_{Du}(S/C) \tag{6.3}$$

Equation (6.3) contains the full blockage/wake-constraint correction and can be solved directly. The blockage constant remained as before, with $C_{D\infty}$ in the right hand side now replaced by the uncorrected, wind-axis drag coefficient, $C_{Du}$, increasing the correction magnitude. The correction is due to the separated-flow component of drag that, in the case of a normal flat plate, is almost the total drag. For other geometries, this may not be the case, and the separated drag component must be estimated for use in equation (6.3). The remaining drag components are treated in the standard fashion. The fully corrected drag coefficient, containing both flow speed increase and drag change due to wake constraint, is denoted by $C_{DcM1}$. The subscript 1 indicates a single-step correction and separates Maskell's original version from a later, two-step interpretation that will be presented in Section 6.2.3.

When the wake-blockage correction is applied to bodies that have drag contributions from other sources than flow separation, then the drag components must be estimated so that Maskell's correction can be applied only to the drag resulting from flow separation. Induced drag and skin friction are excluded. When the wake-blockage correction is to be applied to an aircraft model, for example, it is done as follows,

$$\begin{aligned}\left(\frac{q_c}{q_u}\right) &= \left[1+2\varepsilon_{wa}+2\varepsilon_{ws}\right] \\ &= \left[1+\left(\frac{1}{2}\right)\left(\frac{S}{C}\right)(C_{Dr}+C_{Do})+\theta\left(\frac{S}{C}\right)(C_{Du}-C_{Di}-C_{Do})\right]\end{aligned} \tag{6.4}$$

$\varepsilon_{wa}=(U_{wa}-U_o)/U_o=\Delta U_{wa}/U_o$ is the blockage factor due to the thin, attached-flow wake (classical component) and $\varepsilon_{ws}=\Delta U_{ws}/U_o$ is the velocity increment due to the separated wake (Maskell component). $U_o$ is the upstream reference velocity measurement that is assumed to be unaffected by blockage, $C_{Dr}$ is the support rig drag, $C_{Do}$ is the drag due to skin friction, $C_{Du}$ is the total drag coefficient, and $C_{Di}$ is the induced drag. The last term in parentheses of the right hand side of the equation, $(C_{Du}-C_{Di}-C_{Do})$, is the uncorrected, separated-flow drag, $C_{Dus}$. In the aircraft case, the drag breakdown can be done readily, with due care in accounting for separated flow on flaps. In other applications, such as to automobiles, the drag breakdown is less certain. As a result, the uncorrected drag coefficient is used often instead of $C_{Dus}$ because no other choice is available and because most of the drag is pressure drag due to flow separation.

As will be seen, the correction due to wake constraint should be in the form of a drag increment, rather than a dynamic pressure change. When the correction is recast into this form, an improved correction to drag and to the other aerodynamic forces and moments results. The details of this derivation are presented in Section 6.2.3. Strictly speaking, equations (6.3) and (6.4) are drag coefficient corrections only.

Equation (6.2) can be used to calculate the value of the blockage constant $\theta$, using the corrected, average base pressures measured over the separated region of the model under test or from generic measurements on bluff bodies with similar separated flows.

Maskell obtained $\theta$ as a function of aspect ratio from measurements on normal flat plates and argued that these data could be generalised to other, similar, bubble-type separations. The blockage constant

was found to be within ten percent of $\theta$=2.5 for plates (square plate $C_{pbc} \approx -0.4$) having aspect ratios between 1 and 10.

When base pressure measurements are made, the corrected base pressure coefficient is obtained by iterating the following equation,

$$(1-C_{pbc})_i = \frac{(1-C_{pbu})}{1+(-1/C_{pbc})_{i-1}(C_{Dus}S/C)} \tag{6.5}$$

The measured base pressure is used as the starting point for the iteration. Gould [6] pointed out that the required pressure is the separation pressure coefficient, which is the base pressure coefficient for a flat plate.

The fundamental assumption made by Maskell was that the pressure field was invariant under constraint. Thus, blockage only scales the flow speed. The implication is that flow-separation and flow-reattachment locations must not be changed by wall constraint. Maskell provides evidence of this for the flat plates that were used to determine the empirical constants.

In addition, Farrell et. al. [11] have provided further insight into the effect of constraint on the invariance of the pressure field based on the behaviour of two-dimensional circular cylinders. These authors showed that the pressure rise between the point of maximum suction on the side of a circular cylinder and the base of the cylinder was independent of blockage up to S/C=0.21. This finding suggests that wall constraint has little effect on flow separation on bluff bodies up to this blockage level.

While the derivation of Maskell's correction formula, and the commonly-used values of the blockage constant $\theta$, were based on data from normal flat plates, these values of $\theta$ have been applied to wings with flow separation. The constant for two- and three-dimensional normal flat plates is a function of plate aspect ratio and is fitted by,

$$\theta = 0.96 + 1.94 \exp(-0.06\,AR) \tag{6.6}$$

The variation of equation (6.6) with aspect ratio is compared to Maskell's estimates in Figure 6.3.

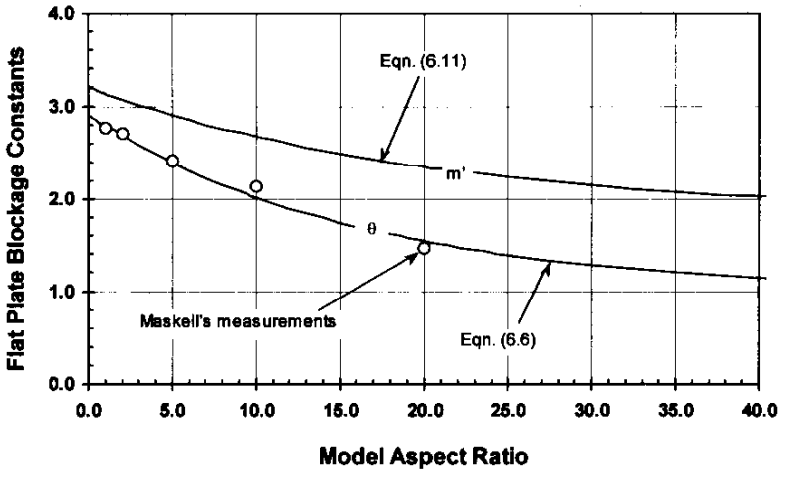


Fig. 6.3: Flat Plate Blockage Constants

The functional relationship implied in the data correlation of Figure 6.2 is that of equation (6.3), with the slope of the curve being $\theta$. The flat-plate data from the closed test sections, Figures 6.1 and 6.2, were measured for aspect ratios between 1 and 3. Maskell's blockage constant takes on values in the range $2.5 \leq \theta \leq 2.8$ for these aspect ratios, which are close to the slopes of 2.53 for the flat-plates and 2.41 for the rectangular blocks in Figure 6.2.

Gould [6] showed that the correction was also valid for floor-mounted plates if the plate was considered as a plate of twice the height reflected about the floor as a plane of symmetry (duplex test section). As a result, the correction should apply equally well to two-dimensional testing, three-dimensional testing, and reflection-plane testing.

Although the correction is expressed as a dynamic pressure adjustment, it is more properly a correction to drag because of its momentum-based derivation. The inclusion of the wake distortion due to boundary constraint has effectively combined the incremental drag correction due to this effect with the dynamic pressure correction. Thus, while drag should be properly corrected, the other forces and moments will be over-corrected because the dynamic pressure correction has too large a value.

### 6.2.2 COWDREY'S DEVELOPMENT

Cowdrey [12] re-derived Maskell's method without the wake distortion effect for three-dimensional bodies that lie in their own wakes (leading-edge separation) and showed that the constant-base-pressure assumption was not required. He produced a correction that did not depend on the measured drag, although it still required an empirical constant that was a function of body geometry. His version of the correction had the form,

$$\left(\frac{q_c}{q_u}\right)=\left(\frac{C_{Du}}{C_{D\infty}}\right)=\frac{1}{1-m(S/C)} \tag{6.7}$$

m is a semi-empirical constant that must be determined by experiment. If equations (6.1) and (6.7) are equated, then it can be seen that,

$$m=-(C_{D\infty}/C_{pbc}) \tag{6.8}$$

Equation (6.7) can also be written as,

$$\left(\frac{q_c}{q_u}\right)=\left(\frac{C_{Du}}{C_{DcMl}}\right)=1+m'(S/C) \tag{6.9}$$

When equation (6.9) is compared to equation (6.3), *which contains the wake constraint effect*, then the blockage factor, m', can be represented by,

$$m'=-(C_{Du}/C_{pbc})=\theta C_{Du} \tag{6.10}$$

An equation for m' for normal flat plates that is equivalent to equation (6.6) previously quoted for $\theta$ can now be written. It is,

$$m'=1.85+1.35\exp(-0.05\,AR) \tag{6.11}$$

Equation (6.11) is shown in Figure 6.3 also.

### 6.2.3 HACKETT'S TWO-STEP VERSION OF MASKELL'S ANALYSIS

Maskell's momentum analysis combined the dynamic pressure and the incremental drag blockage components into a single dynamic pressure adjustment, making it a correction to drag only. Hackett [13, 14] realised this and separated Maskell's correction into its two constituent components, based on the difference between equation (6.3) and equation (6.1). This difference should be an increment in drag,

not a change in dynamic pressure. Hackett defined the drag increment to be $\Delta C_{D_M} = C_{D_{cM1}} - C_{D_\infty}$, which is the difference between the corrected drag coefficients with and without the effect of wake constraint included.

The resulting 'two-step' version of Maskell's analysis should provide a superior adjustment to drag and to the other forces and moments, since the correction is separated into its correct components.

Maskell's correction for separated-flow blockage alone, equation (6.1), was restated by Hackett as,

$$C_{D\infty} = (C_{DcM1} - \Delta C_{DM}) = \frac{C_{Du}}{(q_c / q_u)_1} = \frac{C_{Du}}{1 + \theta(C_{DcM1} - \Delta C_{DM})(S/C)} \tag{6.13}$$

Hackett then re-wrote the blockage correction in terms of a blockage-induced incremental velocity and a drag increment, to produce the following two-step (dynamic pressure and incremental drag) correction,

$$C_{DcM2} = \frac{(C_{Du} + \Delta C_{DM})}{(q_c/q_u)_1} = \frac{(C_{Du} + \Delta C_{DM})}{1 + \theta(C_{DcM1} - \Delta C_{DM})(S/C)} \tag{6.14}$$

$C_{DcM2}$ is the drag coefficient corrected by Hackett's two-step version of Maskell's method. The dynamic pressure correction in the two-step approach, $(q_c / q)_1$, now *does not include* the wake distortion effect, which resides in $\Delta C_{DM}$. $\Delta C_{DM}$ is obtained from the solution of the following quadratic equation, derived by equating $C_{Du}$ in equations (6.3) and (6.13).

$$\Delta C_{DM}^2 - \left(\frac{1}{\theta(S/C)} + 2C_{DcM1}\right)\Delta C_{DM} - C_{DcM1}(C_{Du} - C_{DcM1}) = 0 \tag{6.15a}$$

Only the negative solution to equation (5.15a) is physically valid since $C_{DcM1}$ must be smaller than $C_{D\infty}$.

It is important to note that the expressions presented in [13] and [14] differ, and that the results from [14] are used here. The linear approximation presented in [13] for $\Delta C_{DM}$ is incorrect due to a typographical error in the transactions paper. Further, the correct expression was applicable only for small values of $\varepsilon C_{Du}(S/C)$. These issues are summarised in a discussions presented in the AIAA Journal [15]. In this discussion, Hackett presents the closed-form solution to equation (6.15a) as,

$$\Delta C_{DM} = \frac{C_{Du}}{(1 + \theta C_{Du}(S/C))} + \left[\frac{C_{Du}}{2\theta C_{Du}(S/C)}\right]\left[1 - \sqrt{1 + 4\theta C_{Du}(S/C)}\right] \tag{6.15b}$$

A comparison of Maskell's method [1], Hackett's two-step version [14] and Cowdrey's analysis [12] is provided by applying them to the average fit line through the flat-plate drag coefficients in Figure 6.1. Equations (6.3), (6.7), and (6.14), along with their ancillary relations, were applied as corrections to these data. The results are collected in Figure 6.4. It can be seen that the tendency to over-correction in Maskell's method is removed by use of the two-step derivation of Hackett.

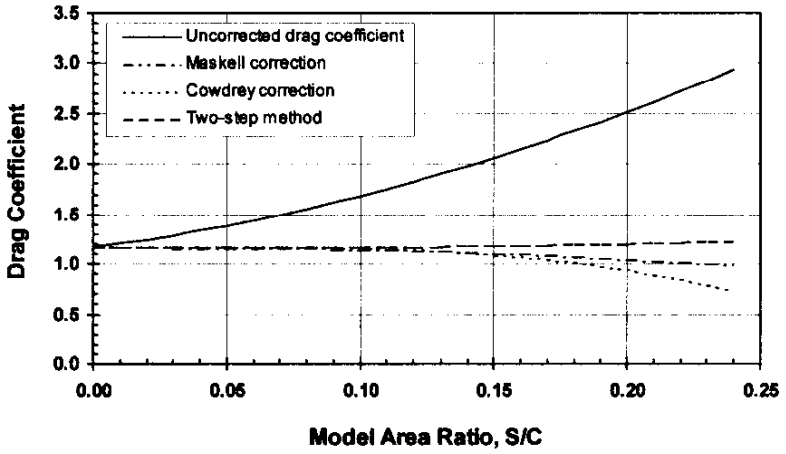


Fig. 6.4: Comparison of Separated-Flow Corrections For Three-Dimensional, Normal Flat Plates [6]

### 6.2.4 COMMENTARY ON MASKELL'S CORRECTION

Maskell's method has been found to over-correct at large area ratios when applied to many two-dimensional and three-dimensional bluff bodies, as demonstrated for two-dimensional rectangular cylinders in [16] and as seen for three-dimensional normal plates in Figure 6.4 [6]. The two-step development of Hackett should remedy this situation, and it would be beneficial to revisit many data sets to verify that this is the case. It would also be expected that the two-step version might be more accurate for aircraft with separated flows.

### 6.2.5 WAKE BUOYANCY AND THE WAKE-INDUCED DRAG INCREMENT

Controversy has arisen over the correct form of the drag increment at the body due to the constraint of the wake of the body by the tunnel walls. The classical adjustment [2], ascribed to buoyancy resulting from a wake-induced pressure gradient (excluding compressibility), is,

$$\Delta C_{Dwb} = -\varepsilon_s C_{Du,vis} = -T\left(\frac{V}{C^{3/2}}\right)C_{Du,vis} \tag{6.16}$$

where $T = (\sqrt{\pi}/2)\tau = 0.36(B/H + H/B)$ and $C_{Du,vis} = C_{Do} + C_{Dus}$ is the viscous component of the drag coefficient.

An alternative to this form has been derived recently by Taylor [17] as,

$$\Delta C_{Dwb} = -(\varepsilon_s + \varepsilon_w)C_{Du,vis} \tag{6.17}$$

It involves both the model volume and the wake blockage. Equations (6.16) and (6.17) express a buoyancy force on the model due to the pressure gradient at the model caused by the wake images. Thus, this form of wake-induced correction is referred to as 'wake buoyancy'.

Hackett [13, 14] has argued that both expressions are wrong because they do not include the cross terms acting between the full set of sources and sinks that approximate the body. The cross-terms cancel the buoyancy-based expression, leaving a new term that is not gradient related. Since Hackett's derivation is not limited to bluff flows, it should be more generally valid.

The new term, which had its origins in Hackett's and Wilsden's pressure-signature correction method [18], has the form,

$$\Delta C_{Dwi} = -C_{Du,vis}^2\left(\frac{S}{4C}\right) \tag{6.18}$$

This equation does not contain volume either implicitly or explicitly, and is a function of the square of drag, whereas equations (6.16) and (6.17) are proportional to drag. The term 'wake-induced drag increment' is used to differentiate Hackett's version from the volume-based, buoyancy form. No direct experimental evidence exists to assist in clarifying this issue although one indirect experimental result can be found that supports the use of equation (6.18).

The relevant item is the flat-plate drag coefficient curve in Figure 6.4, which is a fit of the measured drag coefficients from [6] that are presented in Figure 6.1 as open diamonds. The flat plate is a geometry for which the classical buoyancy-based correction would be zero. Equation (6.15b) was applied to the fitted

curve to calculate the wake-induced drag increments for the plate as a function of area ratio. These drag increments are compared with those estimated from Hackett's expression, equation (6.18), in Figure 6.5 and are seen to be in reasonable agreement.

The issues raised above are not yet settled. Further discussion of them can be found in [15].

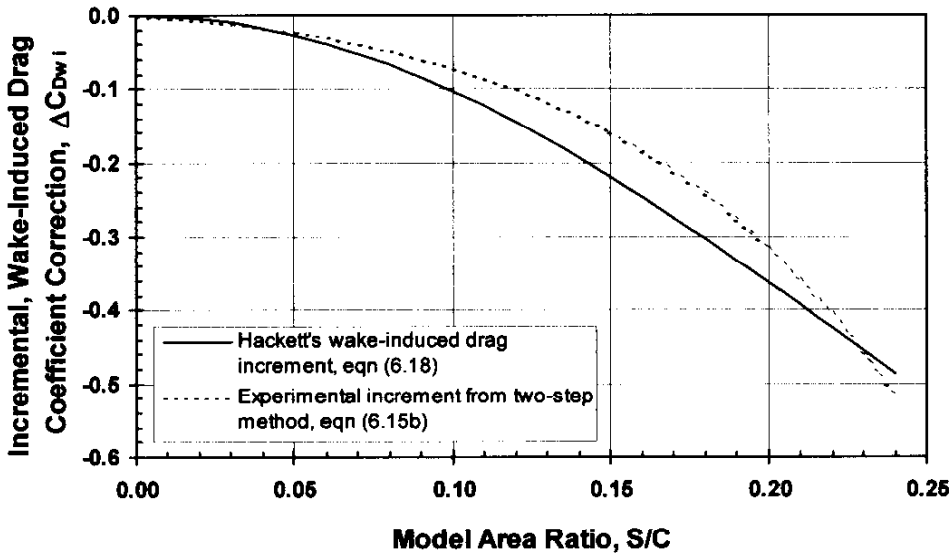


Fig. 6.5: Experimental Verification of Hackett's Wake-Induced Drag Increment For a Flat Plate Perpendicular to the Flow

## 6.2.6 Mercker's Analysis

A blockage correction has been developed by Mercker [19] for application to automotive shapes typified by rear-end flow separation, rather than the front-end separation of sharp-edged bodies. Maskell's constants will not apply to these shapes, although the base-pressure-dependent analysis should still be valid. Mercker's development was based on the solid-blockage analysis of Lock [20] and on the wake-blockage analyses of Maskell [1], Thom [21], and Glauert [22]. The following notation and constants differ from the derivation of [19] only because the correction has been re-written using the duplex test section and duplex model geometries for consistency. The blockage correction has the form,

$$\left(\frac{q_c}{q}\right) = [1+\varepsilon_s+\varepsilon_w]^2$$

$$= \left[1+K\tau\left[\frac{L_p}{\sqrt{F}}\right]\left[\frac{V}{V_t}\right]^{3/2}\left[\frac{F^{3/2}}{V}\right]+\left\{\left(\frac{S}{C}\right)\left[\frac{1}{4}C_{Duo}+\eta\left(\frac{F}{S}\right)+\frac{5}{4}\left(C_{Du}-C_{Di}-C_{Duo}\right)\right]\right\}\right]^2$$

$$= \left[1+K\tau\left[\frac{F}{\sqrt{L_p V}}\right]\left[\frac{V}{C^{3/2}}\right]+\left\{\left(\frac{S}{C}\right)\left[\frac{1}{4}C_{Duo}+\eta\left(\frac{F}{S}\right)+\frac{5}{4}C_{Dus}\right]\right\}\right]^2 \qquad (6.19)$$

where:

$C_{Du}$ = uncorrected, wind-axis drag coefficient at yaw angle $\psi$

$C_{Dus}$ = uncorrected, separated-flow drag coefficient

$C_{Duo}$ = uncorrected, wind-axis drag coefficient at zero yaw angle

$C_{Di}$ = induced drag coefficient at yaw angle $\psi$

$C$ = duplex test-section area = $2C_t$

$L_p$ = projected length of model = $L_m \cos\psi + w_m \sin|\psi|$

$L_m$ = model length

$w_m$ = model width

$\psi$ = yaw angle

$S$ = duplex model frontal area = $2S_m$

$F$ = duplex model projected frontal area = $2(S_m \cos\psi + S_Y \sin|\psi|)$

$S_m$ = model frontal area

$S_Y$ = model side area

$\tau$ = solid blockage constant = $2T/\sqrt{\pi} = 0.41(B/H + H/B)$

$V$ = duplex model volume = $2V_m$

$V_t$ = variable portion of test section volume = $L_p C$

$\eta$ = empirical wake blockage constant determined by Mercker = 0.41

$K$ = empirical solid blockage constant determined by Mercker = 1.0

The term $(S/C)[1/4C_{Duo} + \eta(F/S)] = [1/4C_{Duo}(S/C) + \eta(F/C)]$ effectively contains the wake blockage correction due to both skin friction and flow separation from the base of the bluff shape at zero yaw and small yaw angles. The third term in the curly bracket of equation (6.19) contains the additional separated-flow drag component that occurs at larger yaw angles. This additional separation drag is identified as the portion of the drag coefficient above the linear correlation of $C_D$ versus $\left(C_L^2 + C_Y^2\right)$. Here, an analogy is made to the aircraft drag polar, except that the induced drag is now a function of both lift, $C_L$, and side force, $C_Y$.

The constant value $\eta$=0.41 differs from the value $\eta$=0.43 given in [19] because Mercker re-formulated his method to include the newly-proposed wake-induced-drag increment, equation (6.18). The term in the second line of equation (6.19), pre-multiplying $(V/V_t)^{3/2}$, also differs from that in Mercker's paper due to an improvement made by Mercker. This modification leads to the constant K changing from $(1/\sqrt{\pi})$ in [19] to the value of 1.0 used here.

The correction is applied to drag as,

$$C_{D_c} = \left[\frac{\left(C_{D_u} + \Delta C_{Dwi}\right)}{(q_c/q)}\right] \tag{6.20}$$

where $\Delta C_{Dwi}$ is given by equation (6.18).

### 6.2.7 Upstream and Downstream Effects

Boundary effects upstream and downstream of the model are important also. With more than one model in the test section, the blockage correction at each model will be a combination of the upstream and downstream effects caused by each model. Further, the model's blockage field may distort the reference measurement at the entrance to the test section and the model's flow field may be distorted when the model is too near the end of the test section. These position-in-test-section effects have been studied by Gould [6] and by Garry, Cooper, Fediw, Wallis, and Wilsden [23].

Gould's interest was the blockage interference effects between several axially separated bluff models. He measured the upstream and the downstream variations of the blockage of flat plates in a closed test section. His results showed that the downstream effect was the larger and persisted further. The downstream blockage effect collapsed on distance non-dimensionalised by the mean plate size, expressed as $(x_d/\sqrt{S})$, because the downstream behaviour depends on the size and the development of the viscous wake. The upstream effect was found to collapse on $(x_u/\sqrt{C})$. This behaviour can be ascribed to a potential flow effect, where the mirror image sets of singularities that can be used to describe the blockage have the image separation - the tunnel height and width - as the characteristic dimensions. A reasonable average of these lengths is $\sqrt{C}$ .

The blockage variations with longitudinal position relative to the location of the generating body, as a fraction of the value at the body, are adequately fitted by,

$$\text{upstream effect}: \ (\varepsilon_u/\varepsilon) = \exp\left\{-\left[\frac{\pi}{2}\left(\frac{x}{\sqrt{C}}\right)\right]^2\right\} \tag{6.21}$$

$$\text{downstream effect}: \ (\varepsilon_d/\varepsilon) = 0.3 + 0.7\exp\left\{-0.1\left(\frac{x}{\sqrt{S}}\right)^{1.7}\right\} \tag{6.22}$$

This pair of equations provides the multiplying factor on the blockage induced by a model at a position upstream or downstream of the model. The composite blockage at any location due to several models is the sum of the individual effects. The blockage variations of equations (6.21) and (6.22) are shown in Figure 6.6.

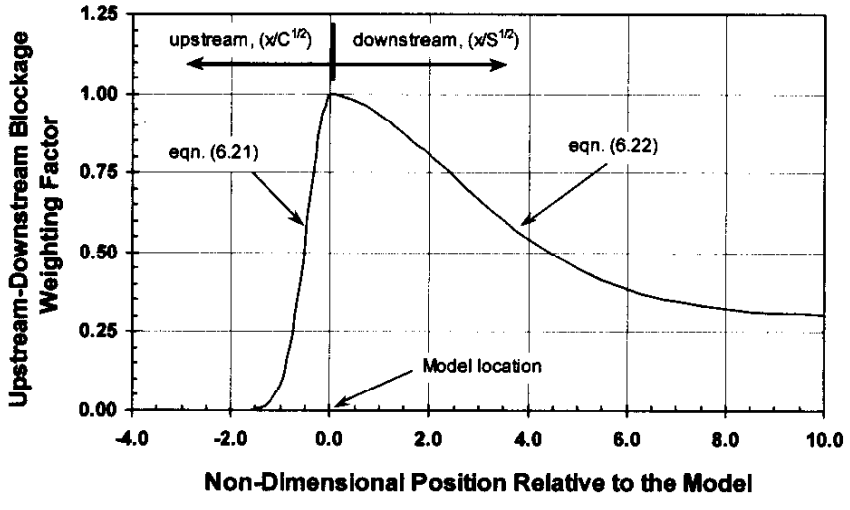


Fig. 6.6: Variation of Blockage Upstream and Downstream of the Model Location [6]

Equation (6.21) indicates that a model should be positioned no closer than $1.5\sqrt{C}$ to the reference static pressure taps to keep the effect of blockage at the taps below one-half percent of the value at the model or no closer than $\sqrt{C}$ to keep the

effect at five percent. Conversely, if the model location is fixed, and if the model blockage can be estimated, then equation (6.21) can be used to determine the error in the reference static pressure measurement.

The authors of [23] were interested in the effect of the proximity of an automobile model to the end of the test section. Here, the end of the test section was defined by the start of the diffuser or the end of a ground board used for improved ground-boundary simulation. Their measurements in three wind tunnels showed a large effect on the drag coefficient due to proximity to the end of the test section. The results suggested that the wake formation region was affected by the diffuser pressure field or by the flow discontinuity at the end of a ground board. In either case, the results were similar - drag was reduced by approximately ten percent. It was found that the drag distortions collapsed on distance from the end of the test section normalised by the square root of the base area, $\sqrt{S_b}$. This area is taken to be the area of the separated region on the base of the model.

Typical base-pressure behaviour as a bluff model approaches the diffuser is seen in Figure 6.7. A large effect on base pressure, and on drag, is seen when the model is too close to the diffuser. Based on these and similar measurements, the authors recommended that models not be positioned closer to the end of a test section than $2\sqrt{S_b}$ and, that whenever possible, models should be at least $4\sqrt{S_b}$ from the end of a test section. These limits should also apply to open-jet tunnels.

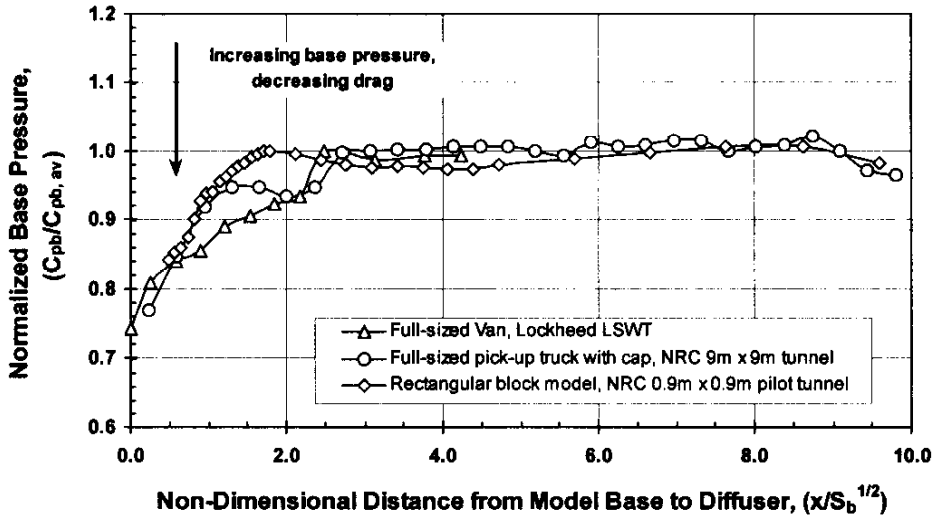


Fig. 6.7: Effect of Proximity of Model Base to Closed-Tunnel Diffuser [23]

## 6.3 METHODS FOR OPEN TEST SECTIONS

The open-jet wind tunnel has classical boundary corrections that are smaller and of opposite sign to those found for closed tunnels [1]. From the classical perspective, the major effect arises from the velocity reduction caused by solid blockage. Here, the jet over-expands, reducing the velocity at the model compared to the upstream measurement. There is no blockage velocity component due to wake blockage because the array of images that provide the free-jet boundary condition are of alternating sign. A correction should be made to drag for this wake constraint. Commonly, these corrections were ignored, as they were considered too small to be of concern.

### 6.3.1 RECENT RESULTS FROM AUTOMOTIVE TESTING

A working group was formed under the auspices of the Society of Automotive Engineers to prepare an Information Report on the boundary corrections used for automotive models in open tunnels [4]. The impetus for this work came from the automotive industry, rather than the aeronautical industry, because many of the world's large open-jet wind tunnels had been designed for the development of automobiles. Correlation studies on identical models in many closed and open full-scale wind tunnels [24] had shown significant differences amongst them.

It was realised that boundary effects for bluff shapes in open tunnels were not negligible, and that the observed behaviour was complex and was not explained by classical theory [4]. For example, comparisons of measurements made on the same full-sized passenger cars [24] and on a family of truck models [25] in open and closed wind tunnels had shown that the closed tunnels consistently measured higher drag coefficients than the open tunnels, even when blockage corrections had been applied. Furthermore, the open tunnel results were not self-consistent.

The classical theories that utilise reflected singularity sets to represent the model and its wake produce an infinitely long free jet. This is not the case in practice, where the jet length is typically 1.5 to 3.0 nozzle hydraulic diameters - limits posed by utility at the lower end and jet stability at the higher end. The finite jet length, not accounted for in the classical theories, is the source of the majority of the important boundary-produced distortions in an open-jet wind tunnel, especially for bluff bodies.

Much of the following discussion is based on the SAE Information Report [4] and on two SAE papers [26,27] written to address the open-jet issues.

### 6.3.2 THE PRIMARY EFFECTS

The situation under consideration is defined in the open-jet test-section schematic of Figure 6.8. A bluff object can create large distortions of the jet that lead to force changes at the body. The majority of these effects result from upstream/downstream constraints imposed by the finite-length jet. The classical representation of the free jet by mirror-image singularities produces an infinite jet and excludes important effects due to the solid wall boundaries at the nozzle and the collector. Mercker and Wiedemann were the first to identify and name the nozzle and the collector effects, and have derived a correction to account for them [26,27]. They grouped the interference effects into four categories. These are:

1. *Nozzle Blockage* – The interference of a model on the nozzle changes the calibration of the dynamic-pressure measuring system from the empty-tunnel value. The distortion is different when using either the nozzle or the plenum reference

pressures. Both reference methods should produce the same result, independent of the model position.

2. *Solid Blockage and Jet Expansion* - A free-jet flow over-expands at the model, reducing the velocity at the model to a value below that measured during the empty-tunnel calibration. Proximity of the model to the nozzle increases this effect.

3. *Empty-Tunnel Pressure Gradients* - Drag changes are caused at the model due to the empty tunnel pressure gradient.

4. *Collector Blockage Effects* - The flow-speed at the model location is changed from the free-air condition due to the constraints on the wake imposed by the collector.

An additional effect due to the wake constraint, similar to the incremental drag correctionin closed tunnels, may also exist.

5. *Wake-Induced Effects* - The solid-wall constraints on the wake as it enters the collector may produce a drag increment at the model.

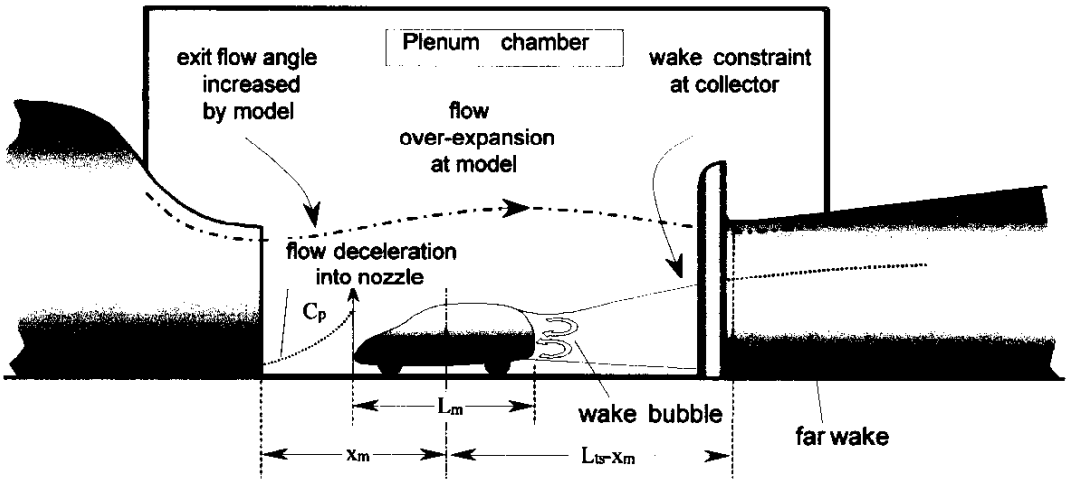


Fig. 6.8: Schematic View of the Open-Jet Wind Tunnel

### 6.3.2.1 NOZZLE BLOCKAGE

The most fundamental blockage effect is Item 1 in the preceding section - the influence of model proximity to the exit plane of the nozzle on the wind tunnel dynamic pressure calibration. The dynamic pressure in an open tunnel is usually measured in one of two ways; using the pressure drop between the settling chamber and the plenum surrounding the jet - the plenum method - or using the pressure drop between the settling chamber and the nozzle - the nozzle method. The nozzle-based measurement is denoted by $q_n$ and the plenum-based measurement is denoted by $q_p$.

When using the nozzle pressure drop, the reference pressure taps in the nozzle should be positioned sufficiently far upstream into the nozzle that they are unaffected by the model. Both pressure drops are calibrated against a reference probe in the empty jet and give an equally good empty-tunnel calibration. The two calibrations change, however, when a model is present in the test section, so that each method provides a different dynamic pressure measurement for the same test condition. The difference between

the two measurements is usually a function of the axial position of a model relative to the nozzle exit plane and of the drag of the model.

Figure 6.9 shows an example of this behaviour through the drag coefficient changes measured by Kuhn [28] on a flat plate as a result of moving the plate upstream toward the nozzle. The drag coefficient based on the nozzle calibration is increasingly higher than that based on the plenum calibration, which is nearly constant with position. This behaviour is caused by model interference on the nozzle flow.

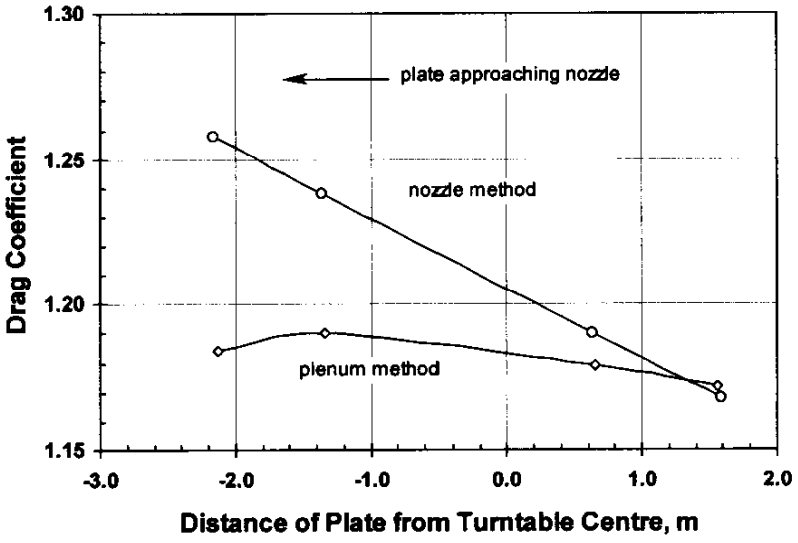


Fig. 6.9: Variation with Axial Position of the Drag Coefficient of a Flat Plate Based on Both the Plenum and the Nozzle Dynamic Pressure Measurements [28]

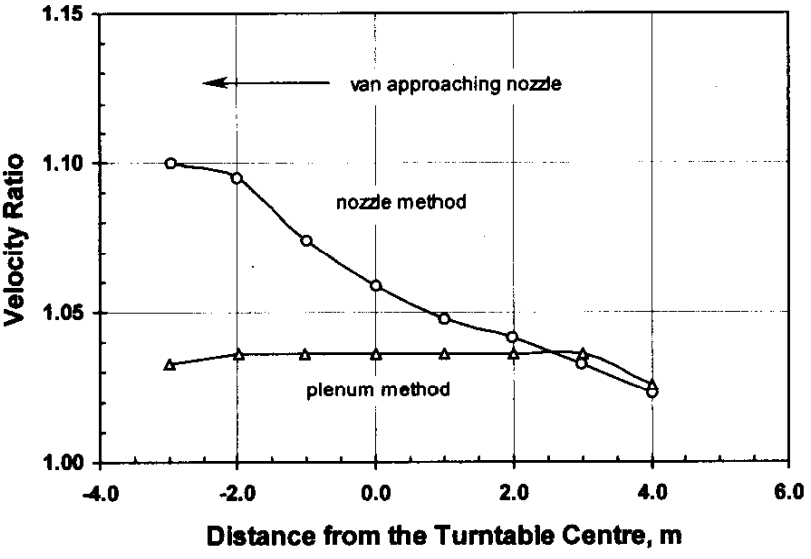


Fig. 6.10: Variation with Axial Position of the Ratio of the Velocity Measured Beside a Van to the Nozzle- and the Plenum-Method Velocities [28]

An explanation of this behaviour is contained in the jet velocity measurements of Figure 6.10 [28]. Here, the velocity beside a van having an area blockage of S/C=0.118 was measured near the edge of the jet by an anemometer and was compared to the plenum-based and the nozzle-based velocity measurements as the van was moved along the test section. The resulting velocity ratios were almost identical when the van was furthest from the nozzle. As the van was moved toward the nozzle, the anemometer velocity measurement increased compared to the nozzle calibration but remained nearly the same as the plenum calibration. Thus, the drag coefficient of a body would increase if based on the nozzle dynamic pressure measurement and would remain approximately constant if based on the plenum measurement, as the model approached the nozzle. This is the behaviour observed for the flat plate.

Figure 6.11 [28] shows that the cause of these velocity variations with van position lies in the effect of the model on the velocity distribution at the nozzle exit plane. The figure presents measurements of the

flow field over the exit plane of the nozzle with a van present in the test section. They are presented as contours of constant velocity ratio, where the measured, nozzle-plane velocities are normalised by the reference velocity obtained using the nozzle method.

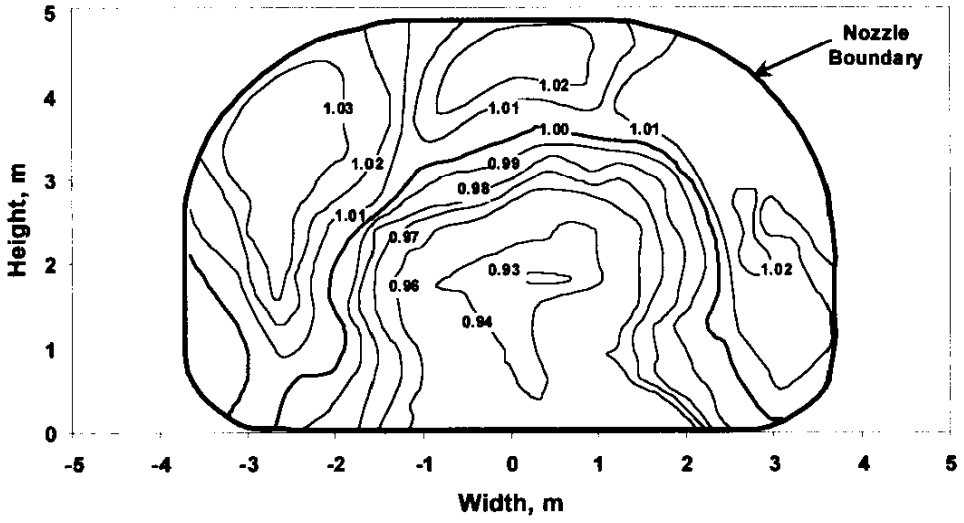


Fig 6.11: Ratio of the Velocity Measured over the Nozzle Exit Plane to the Nozzle-Method Reference Velocity with a Transit Van in the Test Section [28]

The flow deceleration upstream of the van can be seen to extend into the nozzle, producing a non-uniform velocity distribution. The flow velocities near the lower centre of the jet are retarded while the flow velocities around the periphery are accelerated, to satisfy continuity. The same deceleration would occur in free air, minus the closed-wall blockage effect due to the nozzle walls. Effectively, the open jet wind tunnel flow may be subjected to a speed increase similar to that normally associated with a closed tunnel and the reverse of that normally assumed for an open tunnel. The magnitude of this effect would depend on model size and proximity to the nozzle. The closer the model was to the nozzle exit plane, the larger the central speed reductions and the peripheral speed increases would be. The average velocity ratio over the nozzle area in Figure 6.11 is 1.0 because the nozzle method measures the average velocity at the nozzle.

The velocity in the jet periphery is higher than that measured using the nozzle method, by 2 percent to 3 percent, in this case. This increase is similar to the change in velocity ratio between the furthest downstream position of the van and the position of the van during the velocity survey, x = -0.2 m in Figure 6.10. As the van is moved closer to the nozzle, the gradients in velocity over the nozzle would be expected to increase further, leading to the increasing anemometer/nozzle velocity ratio seen in Figure 6.10.

The plenum-based velocity ratio remains nearly fixed because the plenum pressure is equal to the static pressure at the jet boundary and so the plenum-based velocity measurement tracks the velocity increase. As will be shown, neither measurement provides the effective free-stream approach velocity in the plane of the nozzle.

#### 6.3.2.2 SOLID BLOCKAGE AND JET EXPANSION

The classical correction for blockage in an open tunnel [2] is a velocity *reduction* induced by over-expansion of the free-jet flow around the model, compared to the free-air flow. Additionally, as a bluff shape approaches a nozzle, the flow angle is increased by model proximity, further increasing the jet expansion. This effect is characterised in the free-streamline analyses for flat plate models in jet flows presented in Birkhoff, Plesset and Simmons [29], in which the emergent flow angle from a nozzle upstream of a flat plate is shown to increase with the approach of the plate to the nozzle. This expansion effect is not included in the classical, infinite-jet analysis and is more likely to be important for the flows associated with automobiles or trucks than for streamlined aircraft shapes.

#### 6.3.2.3 EMPTY-TUNNEL PRESSURE GRADIENTS

The largest interference effect results from the pressure distribution that exists in the free jet (measured with the model absent) as it flows between nozzle and collector. Changes in the pressure distribution with the model present are dealt with separately, usually as a blockage effect that appears as an increment in drag at the model.

Typical empty-tunnel, axial static pressure distributions show a concave-upward characteristic [4]. The static pressure drops as the jet exits the nozzle, becoming nearly constant over the central region of the jet, generally not at zero pressure coefficient, before rising again as the flow decelerates on approaching the collector. The pressure gradients that occur are large compared to closed tunnels, and extend over the region usually occupied by models. The gradients are not constant over the model, necessitating some form of integration of the pressure distribution over the model for an adequate correction.

#### 6.3.2.4 Collector Effects

There will be additional effects on a bluff model as its large wake enters the collector, going from an open-jet boundary condition to a closed-wall boundary condition. The entry of the bluff-body wake into the collector may result in a closed-wall, wake-induced velocity increment at the model due to the changed constraint on the wake. This effect is a result of the finite jet length and the fact that the model frequently terminates close to the entrance to the collector.

#### 6.3.2.5 WAKE-INDUCED EFFECTS

The wake-induced drag increment for an open tunnel is small. However, as in the previous case, Section 6.3.2.4, wake constraint on entry into the collector may induce a base pressure change at the model in a fashion similar to that for a closed tunnel, Section 6.2.4. No adjustment for such an effect is yet available.

### 6.3.3 THE METHOD OF MERCKER AND WIEDEMANN

Mercker and Wiedemann [26, 27] have identified the major open-jet blockage elements and have developed procedures to correct for their effects. Their first paper [26] clarified the interactions between the model and the nozzle and the model and the diffuser. It corrected the dynamic pressure based on the nozzle-measurement method only. A second paper, by Mercker, Wickern and Wiedemann [27], extended the analysis to include dynamic pressure measurements using either nozzle or plenum measurements. The correction procedure offered a first attempt at analysing the major boundary-induced effects discussed in Section 6.3.2. and provides a framework for further development.

The correction methodology follows standard practice by breaking the boundary-induced effects into a series of components that are combined to provide the full adjustment to dynamic pressure. Following Section 2, the correction to dynamic pressure is written as,

$$\left(\frac{q_c}{q_u}\right) = (1+\varepsilon)^2 = (1+\varepsilon_s+\varepsilon_n+\varepsilon_c)^2 \tag{6.23}$$

The total blockage factor, $\varepsilon = (U_c/U_m) - 1$ is made up of the solid blockage factor $\varepsilon_s$, which is negative, the nozzle blockage factor $\varepsilon_n$, which is positive, and the collector blockage factor, $\varepsilon_c$, which is also positive. $U_c$ is the velocity corrected for blockage and $U_m$ is the velocity measured using either of the two reference methods - $u_n$ or $u_p$. Unlike the classical approach to blockage for the infinitely-long open jet, which reduces dynamic pressure, the new correction terms that arise because of finite jet length - the nozzle and the collector effects - are positive and increase the velocity at the model.

It should be noted that the definition of $\varepsilon$ used here is different than that used in either [26] or [27] and so will result in a different equation for the nozzle blockage, although the correction magnitudes that result are virtually identical.

#### 6.3.3.1 NOZZLE BLOCKAGE

The flow velocity at the periphery of the jet, in the nozzle exit plane, has been found to increase as a model approaches the nozzle [28]. This behaviour results from a solid-wall blockage effect caused by the flow deceleration upstream of the model extending into the nozzle. It is the reverse of the effect usually ascribed to open tunnels.

This model influence at the nozzle is fixed, irrespective of the dynamic-pressure-measuring technique. However, the two measuring techniques commonly employed in open tunnels see this phenomenon differently, requiring two adjustment procedures to give correct and identical reference dynamic pressure measurements. The situation is as sketched in Figure 6.12, which shows the velocity field upstream of a body, in the plane of the nozzle.

Assuming that the approach velocity profile at the nozzle exit plane in the tunnel is similar to that in free air, it can be seen that the 'effective' undisturbed approach velocity, $U_o$, is higher than the velocity measured by either reference method. The difference between the velocity measured at the nozzle, either $U_n$ or $U_p$, and the effective free-stream asymptote, $U_o$, provides the nozzle blockage factors.

The nozzle method measures the average velocity across the nozzle. This value must be increased by a velocity increment equal to ($\varepsilon_{qn}U_n$) to equal the free stream asymptote. Because the plenum method

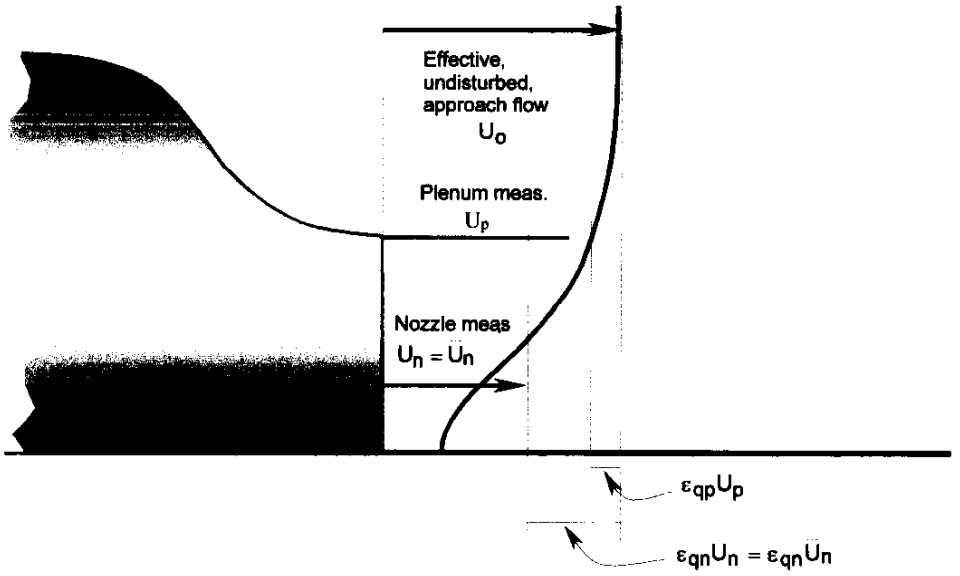


Fig. 6.12: Relationship Between Nozzle and Plenum Measurements and the Equivalent Undisturbed Free-Air Approach Flow

provides the velocity at the jet boundary, a smaller velocity increment is required to raise it to the same free-stream approach flow. This increment is ($\varepsilon_{qp}U_p$).

The derivation of the corrections for flow constraint in the nozzle proceeds through a representation of the upstream effects of the model at the nozzle plane by a simple point source. This source is sized to provide an area of the resulting body of revolution at downstream infinity that is equal to the frontal area of the model. The source is positioned so that the stagnation point on the semi-infinite body of revolution produced by it is located at the leading edge of the vehicle model that it represents.

The source strength is,

$$\left(\frac{Q_s}{U_o}\right) = S \tag{6.24}$$

S is the frontal area of the model for a centrally mounted model, or is twice the frontal area, the duplex model area, for a floor-mounted model such as an automobile. The nozzle area, C, is utilised in the single or the duplex fashion, as appropriate. The distance from the source to the nozzle, measuring positively downstream from the source location (thereby making this distance negative), is,

$$x_s = -x_m + \left(\frac{L_m}{2}\right) - \left(\frac{S}{2\pi}\right)^{1/2} \tag{6.25}$$

where $x_m$ is the distance from the centre of the model to the nozzle (thus the negative sign) and $L_m$ is the length of the model. The location of the stagnation point relative to the source is the last term on the right-hand side of equation (6.25).

*Nozzle Method* - Considering the nozzle-method measurement first, the correction proceeds by computing the average of the horizontal velocity component over the nozzle location, in the presence of the source, as a fraction of the effective approach free-stream velocity at infinity in the plane of the

nozzle, $U_o$. The magnitude of the horizontal velocity component, in cylindrical co-ordinates, with origin at the source location and measuring x positively downstream, is,

$$\left[\frac{U_x(x,r)}{U_o}\right]=\left[\frac{U_o+u_x(x,r)}{U_o}\right]=\left[1+\left(\frac{Q_s}{4\pi U_o}\right)\left(\frac{x}{\left(x^2+r^2\right)^{3/2}}\right)\right] \tag{6.26}$$

where the source strength is given by equation (6.24).

Taking continuity into account, the mean nozzle velocity, $\bar{U}_n$, from which the perturbation velocity at the nozzle can be determined, is obtained by integration of equation (6.26). This integration returns a velocity that is equal to the reference velocity measured by the nozzle method. The mean velocity at the nozzle plane was found to be [26],

$$\left[\frac{\bar{U}_n}{U_o}\right]=\left[1-\left(\frac{S}{2C}\right)\left(1+\frac{x_s}{\left(x_s^2+R_n^2\right)^{1/2}}\right)\right] \tag{6.27}$$

The perturbation velocity at the nozzle plane due to nozzle blockage, when using the nozzle method, is,

$$\varepsilon_{qn}=\left[\frac{U_o}{\bar{U}_n}-1\right]=\frac{\left(\frac{S}{2C}\right)\left(1+\frac{x_s}{\left(x_s^2+R_n^2\right)^{1/2}}\right)}{\left[1-\left(\frac{S}{2C}\right)\left(1+\frac{x_s}{\left(x_s^2+R_n^2\right)^{1/2}}\right)\right]} \tag{6.28}$$

where $R_n=\sqrt{2C_n/\pi}=\sqrt{C/\pi}$ is the hydraulic radius of the duplex nozzle.

A vortex ring positioned at the nozzle exit plane was used to project the blockage factor from the nozzle plane to the model location. The velocity reduction at the model location accounts for the flow relaxation once the solid-walled nozzle constraint is removed as the jet emerges from the nozzle. The circulation of the vortex ring is set to equate the velocity induced by the vortex ring at the centre of the nozzle to the velocity at the same point produced by the upstream effect of the model. The complete expression for the blockage factor at the model due to nozzle blockage becomes,

$$\varepsilon_n=\varepsilon_{qn}\left[\frac{R_n^3}{\left(x_m^2+R_n^2\right)^{3/2}}\right] \tag{6.29}$$

*Plenum Method* – The plenum-method analysis proceeds in a similar fashion, with a blockage correction that is derived from the singularity-based velocity profile. This time, the ratio of the velocity at the edge of the jet to that far away, $(U_p/U_o)$, is required, recognising that the plenum method provides the wind speed at the jet periphery. Using equation (6.26), the ratio of the horizontal component of velocity at the edge of the jet to that far away in an unconstrained flow is,

$$\left[\frac{U_p}{U_o}\right] = \left[\frac{u_x(x_s,R_n)}{U_o}\right]$$

$$= \left[1+\left(\frac{Q_s}{4\pi U_o}\right)\left(\frac{x_s}{\left(x_s^2+R_n^2\right)^{3/2}}\right)\right]^{-1/2}$$

$$= \left[1+\left(\frac{S}{4\pi}\right)\left(\frac{x_s}{\left(x_s^2+R_n^2\right)^{3/2}}\right)\right]^{-1/2} \qquad (6.30)$$

Thus, the blockage factor due to nozzle blockage at the nozzle exit plane, when using the plenum method, is,

$$\varepsilon_{qp} = \left[\frac{U_o}{U_p}-1\right] = \frac{-\left(\frac{S}{4\pi}\right)\left(\frac{x_s}{\left(x_s^2+R_n^2\right)^{3/2}}\right)}{\left[1+\left(\frac{S}{4\pi}\right)\left(\frac{x_s}{\left(x_s^2+R_n^2\right)^{3/2}}\right)\right]} \qquad (6.31)$$

The perturbation velocity obtained from equation (6.30) is smaller than that obtained when using the nozzle method, equation (6.28), although the two flows are identical. Based on momentum considerations, the authors converted the plenum velocity to the average nozzle velocity through the assumed upstream profile to ensure that both measuring methods, and their corrections, produced the same velocity at the model. For small $\varepsilon$, this results in,

$$\varepsilon_p = \varepsilon_{qp} + \varepsilon_n - \varepsilon_{qn} \qquad (6.32)$$

### 6.3.3.2 Solid Blockage and Jet Expansion

The solid blockage term utilised is the classical form, modified to include an additional jet expansion due to model proximity re-directing the flow from the nozzle, causing the exit flow angle to increase. It has the form,

$$\varepsilon_s = \tau\left(\frac{V}{L}\right)^{1/2}\left(\frac{S}{C_e^{3/2}}\right) \qquad (6.33)$$

where V is the model volume, L is the model length, S is the reference area, and $C_e$ is the 'effective' nozzle area that contains the additional jet expansion (jet deflection) effect due to proximity of the model to the nozzle. $\tau$ is the appropriate constant from [2]. The reduced nozzle effective area approximates the

additional velocity reduction at the model due to jet deflection caused by model proximity to the nozzle. The area reduction was related to the nozzle blockage, and was calculated from,

$$C_e = C/(1+\varepsilon_{qn}) \tag{6.34}$$

where $\varepsilon_{qn}$ is the nozzle blockage defined in equation (6.28). $\varepsilon_s$ is negative, due to the sign of $\tau$, reducing the velocity at the model.

### 6.3.3.3 Empty-Tunnel Pressure Gradients

The pressure distributions in an open-jet tunnel are often non-uniform over the model location. Thus, it is necessary to integrate the pressure gradient over the body under test to achieve an adequate correction for the pressure distribution present. The horizontal buoyancy force acting on a body in a pressure gradient is given by,

$$F_H = \int p\,da = \int (\partial p/\partial x)\,dV \tag{6.35}$$

A simplification to the full integration that was suggested by Mercker and Wiedemann [26] was the replacement of the volume integral by a linear approximation applied separately over the front and the rear halves of the model. The following horizontal-buoyancy correction to drag due to the empty-tunnel pressure distribution resulted,

$$\Delta C_{D_{HB}} = \left[\frac{(V_e/2)}{S}\right]\left[\left(\frac{dC_p}{dx}\right)_n + \left(\frac{dC_p}{dx}\right)_c\right] \tag{6.36}$$

The subscripts n and c refer to the pressure gradients over the front and the rear halves (nozzle and collector ends) of the model, respectively. The use of an effective volume follows the classical works of Munk [30] and Glauert [22], which suggested that the effective volume was greater than the true model volume. The multiplying factor was found to be 1.5 for a sphere and 2.0 for an axial cylinder. A reasonable mid-range value of $V_e = 1.75V$ was chosen for automotive applications. The volume and the area are the single or duplex values for central or wall-mounted models, respectively.

### 6.3.3.4 Collector Effects

Another solid-wall blockage effect was postulated to occur at the end of the test section, as the wake of the model flowed into the collector. The wake is then subject to a solid-wall blockage effect that is felt in a diminished fashion at the model. The blockage effect to which the wake was subject was taken as that derived for an automotive wake based on the analysis of Mercker [19] that was presented for solid wall tunnels in Section 6.2.6. The far-field effect was achieved by projecting the effect at the collector to the model location using the ring vortex model previously employed, with the ring vortex now positioned at the collector.

The wake-blockage factor in the collector throat is given by the small-yaw-angle component of the wake blockage from equation (6.19), which is,

$$\varepsilon_{wc} = \frac{C_{Duo}}{4}\left(\frac{S}{C_c}\right) + 0.41\left(\frac{F}{C_c}\right) \tag{6.37}$$

$C_c$ is the single or duplex collector throat area, F is the single or duplex projected frontal area and the empirical constant 0.41 is that given in Section 6.2.6 for bodies with rear-end separations, like automobiles. Bodies with increased separation at yaw angles greater than 15 degrees would require the full wake blockage correction, equation (6.19).

When the wake separation bubble is small, as for some fast-back cars, the wake-bubble term, 0.41, can be neglected, leaving only the first term in parentheses in equation (6.37).

The collector blockage at the model, using the ring-vortex model, is found to be,

$$\varepsilon_c = \varepsilon_{wc}\left[\frac{R_c^3}{\left[(L_{ts} - x_m)^2 + R_c^2\right]^{3/2}}\right] \tag{6.38}$$

where $R_c$ is the hydraulic radius of the single or duplex collector throat, $L_{ts}$ is the length of the test section, and $(L_{ts} - x_m)$ is the distance from the model centre to the collector throat.

### 6.3.3.5 APPLICATION OF THE OPEN-JET CORRECTION FORMULAE

The corrections to dynamic pressure and drag for all the effects discussed for the open tunnel are:

*Nozzle measurement –*

1. Dynamic pressure, $$(q_c / q_n) = (1 + \varepsilon_s + \varepsilon_c + \varepsilon_n)^2 \tag{6.39}$$

2. Wind-axis drag coefficient, $$C_{Dc} = \frac{\left[\, D/(q_n S_m)\right] + \Delta C_{D_{HB}}}{(q_c / q_n)} \tag{6.40}$$

The remaining forces and moments are corrected using equation (6.39).

*Plenum Method –*

1. Dynamic pressure, $$(q_c / q_p) = (1 + \varepsilon_s + \varepsilon_c + \varepsilon_p)^2 \approx (1 + \varepsilon_s + \varepsilon_c + \varepsilon_n + \varepsilon_{qp} - \varepsilon_{qn})^2 \tag{6.41}$$

2. Wind-axis drag coefficient, $$C_{Dc} = \frac{\left[\, D/(q_p S_m)\right] + \Delta C_{D_{HB}}}{(q_c / q_p)} \tag{6.42}$$

## 6.4 APPLICATION TO CLOSED TEST SECTIONS

### 6.4.1 AIRCRAFT

An example of the application of Hackett's two-step version of Maskell's correction procedure through the stall is presented in Figure 6.13. The measurements were made by Shindo [31] to support the simplified correction method that he had proposed using models of 0.016 and 0.16 area ratio. Only the two-step correction is shown because it and Maskell produced nearly identical corrections. For example, at the highest drag level for the larger model where $C_{Du} = 0.7072$, Maskell provided a dynamic-pressure correction factor of 1.232 while Hackett's two-step method gave a dynamic-pressure correction factor of 1.212 and a drag increment of $\Delta C_{DM} = -0.0126$. Both corrections gave corrected drag coefficients within one count of each other. The lift coefficient corrections were different by the ratios of the dynamic-pressure correction factors.

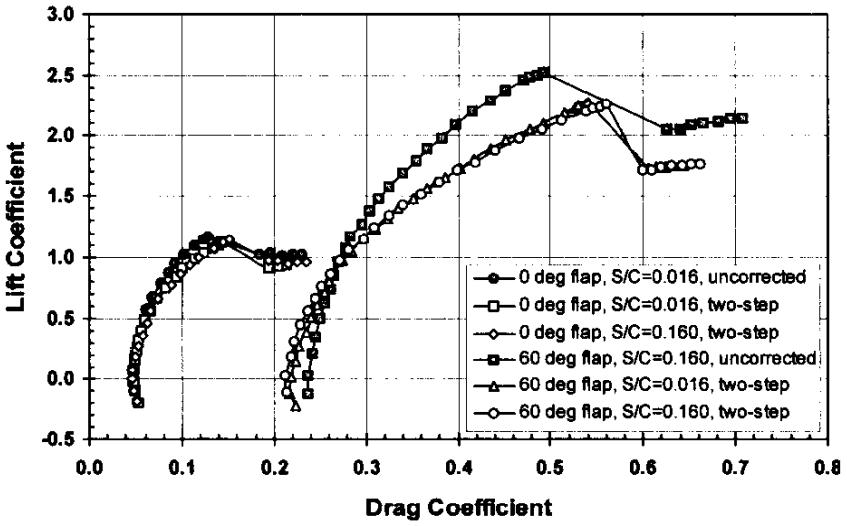


Fig. 6.13: Application of Hackett's Two-Step Version of Maskell's Method to Lift and Drag Measurements on a Rectangular Wing [31]

### 6.4.2 SURFACE VEHICLES

An example of the application of Mercker's method to a simple, rectangular-block automotive shape [8] near the ground is presented in Figure 6.14. Data from two versions of the model are shown - the low-drag model having rounded leading edges and attached front-end flow and the high-drag model having slightly bevelled front edges and a front-edge separation. It can be seen that the correction is not perfect, but that this method agrees well with a correction based on ceiling pressure measurements developed by Hackett, Wilsden and Lilley [18]. The residual error with increasing blockage may have resulted from non-blockage differences in the models or their test installation.

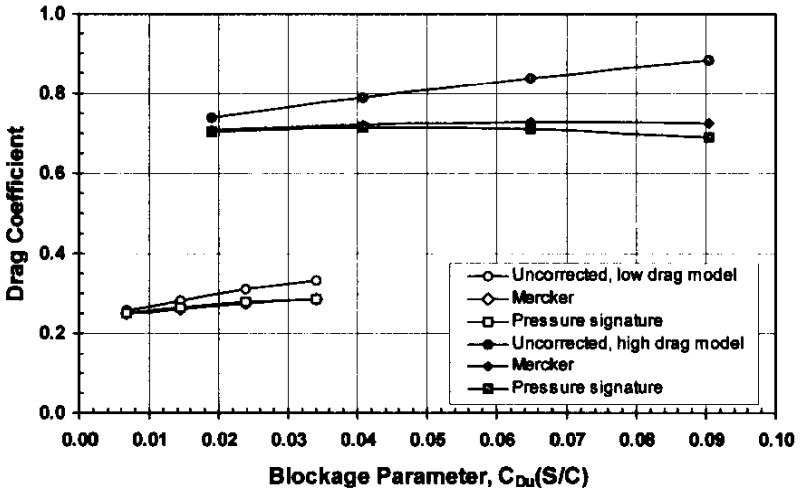


Fig. 6.14: Application of Mercker's Solid-Wall Correction to Bluff Automotive Shapes Near the Ground at Zero Yaw Angle [8]

### 6.4.3 MISCELLANEOUS

A final example is provided by measurements on parachutes made by Macha and Buffington [32] in six different wind tunnels. The authors found that Maskell's empirical blockage constant of $\theta$=2.5 was too large, overcorrecting the measurements. A more appropriate value of $\theta$=1.85 was found by fitting the data. The use of the two-step method returned nearly the same result as the adjusted constant, improving the correction, as seen in Figure 6.15.

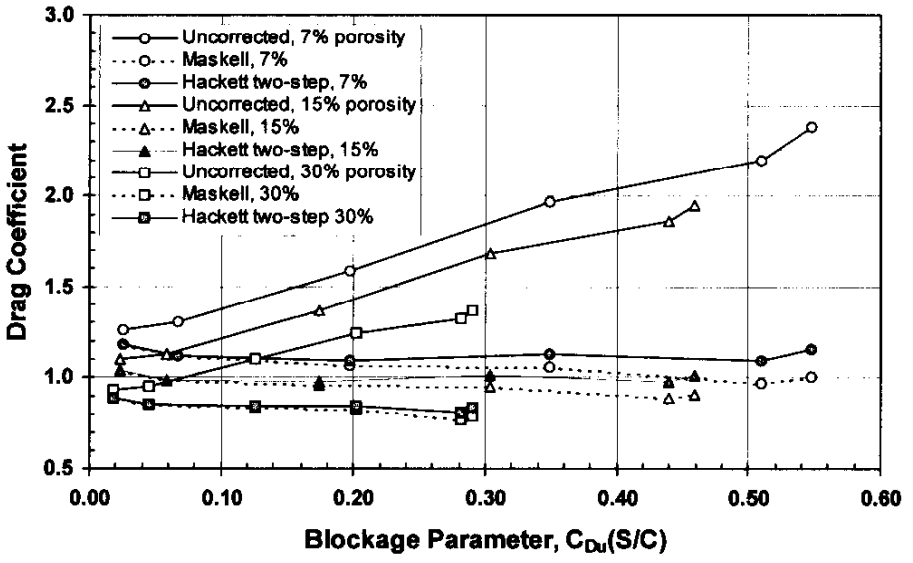


Fig. 6.15: Comparison of Maskell's Method and Hackett's Two-Step Version Using Measurements on Parachutes [32]

## 6.5 APPLICATION TO OPEN TEST SECTIONS

### 6.5.1 SURFACE VEHICLES

The open tunnel correction has been recently developed. It is supported by the data presented by Mercker and Wiedemann [26,27] based on measurements on a full-scale automobile in a series of open and closed wind tunnels. These measurements had initially shown different drag coefficients in the various open wind tunnels. Further, the drag coefficients measured in the open wind tunnels were lower than the measurements from the closed tunnels, even when the closed tunnel results were corrected for blockage. The application of the open-tunnel correction procedure reduced the differences between the open tunnels and brought the results from the open and the closed tunnels into close agreement.

Another example is provided through measurements of the variation with longitudinal position of the aerodynamic drag of a passenger car and a van, made by Mercedes-Benz in their 32.6 $m^2$ open-jet wind tunnel [33]. The sedan and van had area ratios of 0.065 and 0.116, respectively. The reference dynamic pressure was measured using both the nozzle and the plenum methods. Each method resulted in significantly different drag coefficients and both methods produced drag coefficient curves that had large slopes with longitudinal position. These trends can be seen in Figure 6.16. The bumpers of the vehicles were at the exit plane of the nozzle at the furthest upstream positions.

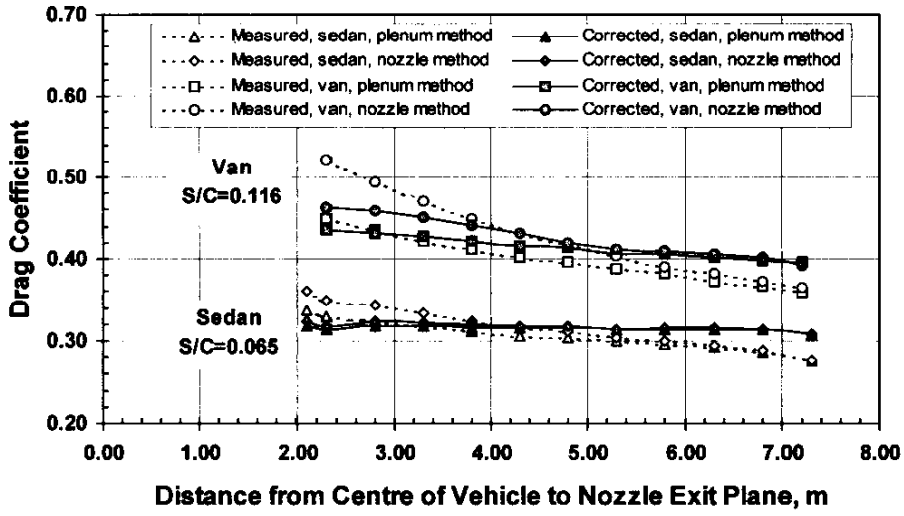


Fig. 6.16: Capability of Mercker's and Wiedemann's Open-Jet Correction [27] For Automotive Models

The application of Mercker and Wiedemann's correction produced almost horizontal drag coefficient curves with changing position for the sedan that were nearly identical for both dynamic-pressure-measuring methods. The correction was not as successful with the higher-blockage van where the corrected drag coefficient curves had residual gradients with position and the curves for the two dynamic-pressure-measuring methods were different. These differences were smaller after correction, however, at the normal 4.8 m measuring location, demonstrating that the method produced a significant improvement in the data. It was possible, that the large, high drag van interfered with the reference static taps.

## 6.6 REFERENCES


[1] E.C. Maskell; A Theory of the Blockage Effects on Bluff Bodies and Stalled Wings in a Closed Wind Tunnel. ARC R&M No. 3400, HMSO, London, Nov. 1965.

[2] H. C. Garner, E. W. E. Rogers, W. E. A. Acum and E. C. Maskell; Subsonic Wind Tunnel Wall Corrections. AGARDograph 109, Paris, France, Oct. 1966.

[3] F. K. v. Schulz-Hausmann, J.-D. Vagt; Influence of Test Section Length and Collector Area on Measurements in ¾-Open-Jet Wind Tunnels. SAE 880251, Society of Automotive Engineers, Detroit, MI, USA, Feb. 1988.

[4] Aerodynamic Testing of Road Vehicles – Open Throat Wind Tunnel Adjustment. SAE Surface Vehicle Information Report J2071, Society of Automotive Engineers, Warrendale, PA, USA, 1994.

[5] T.B. Owen; Measured Blockage Effects on Bluff Bodies in Closed and Open Wind Tunnels. RAE Technical Report 78151, HMSO, London, UK, Dec. 1978.

[6] R.W.F. Gould; Wake Blockage Corrections in a Closed Wind Tunnel for One or Two Wall-Mounted Models Subject to Separated Flow. Aeronautical Research Council R.&M. No. 3649, HMSO, London, UK, 1970.

[7] C. Kramer, H. J. Gerhardt, B. Regenscheit; Wind Tunnels in Industrial Aerodynamics. Journal of Wind Engineering and Industrial Aerodynamics, 16 (1984) 225-264, Elsevier Science Publishers B.V., Amsterdam, the Netherlands.

[8] Closed-Test-Section Wind Tunnel Blockage Corrections for Road Vehicles. SAE SP-1176, Society of Automotive Engineers, Warrendale, PA, USA, Jan. 1996.

[9] Blockage Corrections for Bluff Bodies in Confined Flows. Engineering Sciences Data Item No. 80024, ESDU, London, UK, Nov. 1980.

[10] R. Fail, J.A. Lawford, R.C.W. Eyre Low Speed Experiments on the Wake Characteristics of Flat Plates Normal to an Airstream. ARC R.&M. 3120, June 1957.

[11] C. Farell, O. Guven, S. Carrasquel and V.C. Patel; Effect of Wind-Tunnel Walls on the Flow Past Circular Cylinders and Cooling Tower Models. The American Society of Mechanical Engineers. 1977.

[12] F. Cowdrey; Two Topics of Interest in Experimental Industrial Aerodynamics – Part 1: Application of Maskell's Theory of Wind-Tunnel Blockage to Some Large Models. Part 2: Design of Velocity-Profile Grids. NPL Aero Report 1268, April 1968. Presented at the Symposium on Wind Effects on Buildings and Structures, Loughborough University of Technology, Loughborough, UK, April 1968.

[13] J. E. Hackett; Tunnel-Induced Gradients and Their Effect on Drag. Paper 96-0562, AIAA 34th Aerospace Sciences Meeting, Reno, NV, Jan. 1996. AIAA Transactions, Vol. 34, No. 12, December 1996.

[14] J. E. Hackett; Tunnel-Induced Gradients and Their Effect on Drag. Lockheed Corporation, LG83ER0108, Smyrna, GA, USA, Sept. 1994.

[15] AIAA Journal, Feb., 1998.

[16] J. Courchesne, A. Laneville; A Comparison of Correction Methods in the Evaluation of Drag Coefficient Measurements for Two-Dimensional Rectangular Cylinders. Journal of Fluids Engineering 79-WA/FE-3, 1979.

[17] R. Taylor; Some Fundamental Concepts in the Theory of Wind-Tunnel Wall Constraint and its Applications. Defence Research Agency, DRA/AS/HWA/TR96055/1, Farnborough, UK, June 1996.

[18] J. E. Hackett, D. J. Wilsden, and D. E. Lilley; Estimation of Tunnel Blockage from Wall Pressure Signatures: A Review and Data Correlation. NASA CR-152,241, March 1979.

[19] E. Mercker; A Blockage Correction for Automotive Testing in a Wind Tunnel with Closed Test Section. Journal of Wind Engineering & Industrial Aerodynamics. 1986.

[20] N. H. Lock; The Interference of a Wind Tunnel on a Symmetrical Body. ARC R&M 1275, 1929.

[21] A. Thom; Blockage Corrections in a Closed High Speed Wind Tunnel. ARC R&M 2033, 1943.

[22] H. Glauert; Wind Tunnel Interference on Wings, Bodies and Airscrews. ARC R&M 1566, 1933.

[23] K. P. Garry, K. R. Cooper, A. Fediw, S. B. Wallis, and D. J. Wilsden; The Effect on Aerodynamic Drag of the Longitudinal Position of a Road Vehicle Model in a Wind Tunnel Test Section. SAE 940414, Society of Automotive Engineers, Detroit, MI, USA, Feb. 1994.

[24] R. Buchheim, R. Unger, P. Jousserandot, E. Mercker, Y. Nishimura, F. K. Schenkel, D. J. Wilsden: Comparison Tests Between Major European and North American Automotive Wind Tunnels. SAE 830301, Society of Automotive Engineers, Detroit, MI, USA, Feb. 1983.

[25] K. R. Cooper, H. J. Gerhardt, R. Whitbread, K. P. Garry, G. W. Carr; A Comparison of Aerodynamic Drag Measurements on Model Trucks in Closed-Jet and Open-Jet Wind Tunnels. Journal of Wind Engineering and Industrial Aerodynamics, 22 (1986) 299-316, Elsevier Science Publishers B.V., Amsterdam, The Netherlands.

[26] E. Mercker, J. Wiedemann; On the Correction of Interference Effects in Open Jet Wind Tunnels. SAE 96061, Society of Automotive Engineers, Detroit, MI, USA, Feb. 1996.

[27] E. Mercker, G. Wickern and J. Wiedemann; Views on Nozzle Interference Effects in Open Jet Wind Tunnels. SAE 970136, Society of Automotive Engineers, Detroit, MI, USA, Feb. 1997.

[28] A. Kuhn; Ermittlung der Anströmgeschwindigkeit und der effektiven Windgeschwindigkeit in ¾-offen Fahrzeugwindkanälen. ATZ Automobiltechnische Zeitschrift 97 (1995) 2, Germany.

[29] G. Birkhoff, M. Plesset, and N. Simmons; Wall Effects in Cavity Flow - I. Q. Appl. Math., 8, 2, 1950.

[30] M. Munk; Some New Aerodynamic Relations. NACA Report 114, 1921.

[31] S. Shindo; Simplified Tunnel Correction Method. Journal of Aircraft, Vol. 32, No. 1. January 1994.

[32] J. M. Macha, R. J. Buffington; An Experimental Investigation of Wall-Interference Effects for Parachutes in Closed Wind Tunnels. Sandia Report SAND89-1485, Sandia National Laboratories, Albuquerque, NM, USA, Dec. 1985.

[33] B. Schwartekopp; Private communication. Daimler-Benz wind tunnel data presented at SAE Subcommittee No. 9, Stuttgart Germany, April 1997.